A Novel Method for Removing the Cyclic Frequency Shift due to the Earth's Motion about the Sun from Astronomical Continuous-Wave Data

Curtis Rau[1,2], Colin Gordon[1,2], David Witalka[1,2], and Samuel Akwei-Sekyere[1,3]

Department of Mathematics[1]
Department of Physics and Astronomy[2]
Neuroscience Program[3]
Michigan State University

This senior thesis is presented to Michigan State University for partial fulfillment of the requirements for a baccalaureate degrees in Physics and Neuroscience. In this paper we will introduce the Gustafson Algorithm for removing frequency/phase modulation form a signal. This method is powerful because it works in the frequency rather than time domain (explain why this is an advantage). Here we will focus on its applications to LIGO, but there are many applications. Some other examples are: -Radio wave astronomy -Comunications systems using FM? -What are some other possible applications??

-we are given time series data. -we are looking for phase modulated gravitational waves. -form of phase modulation depends on the nature of the binary orbit. [5] [2] [1] [3] [4]

DIVISION OF LABOR

Curtis Rau

- organized topics and problems of interest, directed group research

- wrote algorithm and discussion of results

- made figures for presentation and paper

- wrote rough draft and template for paper

- Wrote the C++ implementation

Colin Gordon

- researched and solved phase modulation of astronomical signal caused by rotation of earth using circular orbit approximation

- wrote parts of the introduction

- reviewed paper and edited

David Witalka

- created and organized presentation slides

- researched and edited sections on sampling theorem, Nyquist Frequency and aliasing, Carson's rule

- reviewed paper and edited

Samuel Akwei-Sekyere

- reviewed and expanded paper (all sections)

- researched and wrote sections on error analysis, wrote parts of the introduction

I. INTRODUCTION

As a consequence of Einstein's Theory of General Relativity [], it has been postulated that information about the spatial distribution of matter in the universe is transmitted via a gravitational field. From a theoretical standpoint, gravitational waves are manifested in the form of detectable ripples within the fabric of space and time, by changes in gravitational field and as a function of the movement of masses.

Recently, the Laser Interferometer Gravitational-Wave Observatory (LIGO) confirmed the first experimental evidence of gravitational waves. The discovered ripples in space-time by LIGO was a function of the inspiral of two black holes that eventually merged — an even that consumed approximately 30 solar masses. It is believed that gravitational wave sources are actually fairly common in the universe and sources of continuous monochromatic (single frequency) gravitational radiation are predicted to exist — at least sources with frequencies that persist over many periods []. Neutron stars have also been implicated as one of the prime sources of gravitational waves. These stars are expected to emit single frequency waves over long periods of time. Additionally, it has also been proposed that an appreciable fraction of detectable gravitational waves are binary neutron star systems — two neutron starts orbiting around each other.

A fundamental challenge to efficient detection of gravitational waves is that orbiting binary neutron star systems invoke frequency modulations which reduce the power of the carrier frequency and distributes it to higher and lower harmonics. In essence, the power of the signal is dispersed over a range of side-band frequencies; this phenomenon is due to the Doppler effect arising from the Earth's motion relative to the source of the wave. Since the noise observed in the LIGO data is approximately Gaussian and of low signal-to-noise ratio, the extraction of reliable information about gravitational waves is arduous.

In order to calculate the carrier frequency of the wave, consider the wave as one emitted from a source that is megaparsecs away (potentially in other galaxies). By virtue of its distance, the spherical coordinates will not change significantly and the source will move relative to the sun with nearly constant velocity over the time we collect data. By the same token, the sun will experience the monochromatic wave produced by the source as truly monochromatic, while its detection on the Earth will be in the form of a frequency modulated signal.
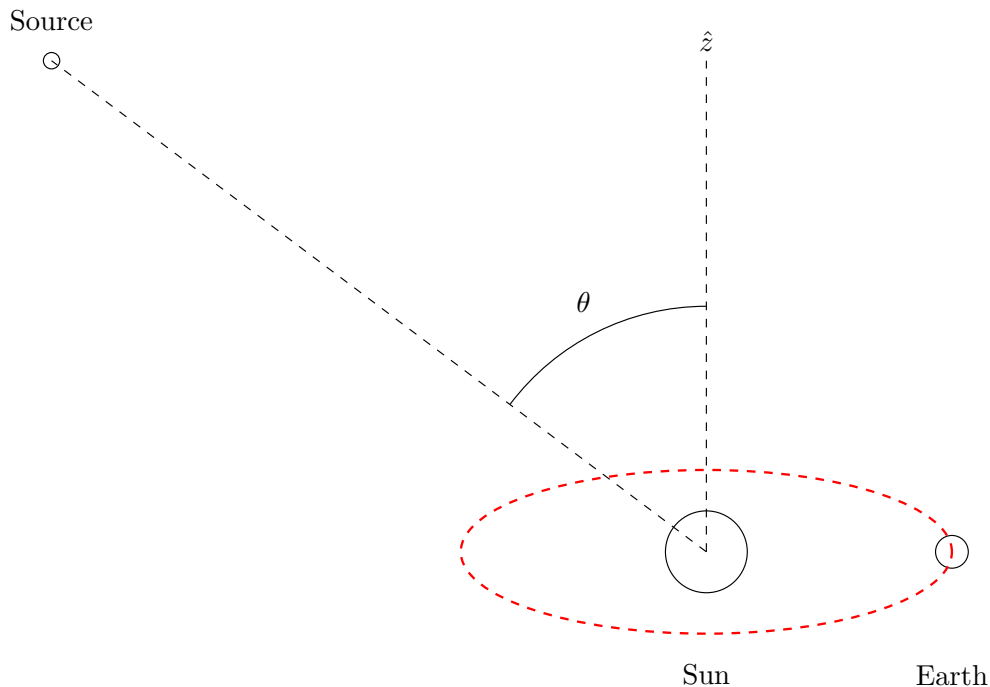

FIG. 1

By assuming that the wave travels at the speed of light, we can capture it as a Lorentz invariant 4-vector with the carrier frequency being the first entry and the second through fourth entries is the wave number. In order to transform it in the Earth's frame we apply an instantaneous Lorentz boost on the 4-vector; the instantaneous boost takes the direction of the motion of the Earth and the velocity of the the Earth in orbit into consideration. Without loss of generality, the Earth's orbit is captured in the xy plane. The 4-vector is written in the perspective that assumes the wave is a plane wave which travels towards the Sun on a trajectory that is on the xz plane. The

matrix with the trigonometric functions projects that 4-vector on a new basis and effectively forcing the second component of the 4-vector to be in the direction of motion of Earth. The matrix with the Betas and gammas is a lorentz transformation that applies on 1st and 2nd component. now the 4 vector is in the frame of the Earth. After all of this, we could apply rotations or whatever to change the spatial coordinate system but we only care about the frequency which is invariant under any of those changes.

$$\mathbf{K} = \begin{pmatrix} \gamma & -\gamma\beta & 0 & 0 \\ -\gamma\beta & \gamma & 0 & 0 \\ 0 & 0 & 1 & 0 \\ 0 & 0 & 0 & 1 \end{pmatrix} \begin{pmatrix} 1 & 0 & 0 & 0 \\ 0 & -\sin(\omega_e t + \phi_e) & \cos(\omega_e t + \phi_e) & 0 \\ 0 & -\cos(\omega_e t + \phi_e) & -\sin(\omega_e t + \phi_e) & 0 \\ 0 & 0 & 0 & 1 \end{pmatrix} \begin{pmatrix} \omega_0/c \\ -k\sin\theta \\ 0 \\ -k\cos\theta \end{pmatrix} \tag{1}$$

$$= \begin{pmatrix} \gamma\left(\omega_0/c - \beta k \sin\theta \sin(\omega_e t + \phi_e)\right) \\ \gamma\left(-\beta\omega_0/c + k \sin\theta \sin(\omega_e t + \phi_e)\right) \\ \gamma k \sin\theta \cos(\omega_e t + \phi_e) \\ -k\cos\theta \end{pmatrix}, \tag{2}$$

where θ is the polar angle from the axis perpendicular to the orbit of Earth, γ is the Lorentz factor from special relativity, ω_e is the angular frequency of the Earth's rotation about the Sun, c is the speed of light and β is the velocity of Earth's orbit divided by the speed of light.

From this formulation we can infer that the new instantaneous frequency in the Earth's frame can be given by:

$$\omega(t) = \omega_0\gamma\left(1 - \beta\sin\theta\sin(\omega_e t + \phi_e)\right). \tag{3}$$

Since the phase refers to the time integral of the frequency, the expression for the wave being sought after is the real part of the following:

$$h(t) = h_0 e^{i\left(\omega' t + \Gamma\cos(\omega_e t + \phi_e)\right)} \tag{4}$$

$$\omega' = \gamma\omega_0 \tag{5}$$

$$\Gamma = \frac{\gamma\beta\omega_0\sin\theta}{\omega_e} \tag{6}$$

where h_0 is the amplitude of the wave, Γ is the modulation index, ω_0 is the frequency of the wave to be detected, ϕ_0 is the phase of the wave to be detected at $t = 0$, ϕ_e is the relative phase difference between the Earth's rotation about the Sun and the wave to be detected.

II. THE GUSTAFSON ALGORITHM

Since the approach is not restricted to gravitational waves and could be detected on another planet other than the Earth, we shall consider a generalized form of the problem. The goal of this paper is to design an algorithm that extracts ω_0, ω_1, Γ, h_0 and ϕ_1 by providing a delta-function as an output if all of the parameters of $f(t)$ being searched for are correct:

$$h_0 e^{i(\omega_0 t + \phi_0 + \Gamma\cos(\omega_1 t + \phi_1))} \rightarrow h_0\delta(\omega_0)\delta(\omega_1)\delta(\Gamma)\delta(\phi_1), \tag{7}$$

where $f(t)$ is the data recorded (as shown below), ω_0 is the frequency of the wave, ω_1 is the angular frequency of the recording site about the Sun, ϕ_0 is the phase of the wave, ϕ_1 is the relative phase difference between the recording site's rotation about the Sun and the wave, Γ is the modulation index and h_0 is the amplitude of the wave.

Previous methods have utilized, asdf.

$$h_0 e^{i(\omega_0 t + \phi_0 + \Gamma\cos(\omega_1 t + \phi_1))} = f(t) \tag{8}$$

$$h_0 e^{i\phi_0} e^{i\omega_0 t} = f(t) e^{-i\Gamma\cos(\omega_1 t + \phi_1)} \tag{9}$$

$$h_0 e^{i\phi_0} \mathcal{F}_t\left[e^{i\omega_0 t}\right] = \mathcal{F}_t\left[f(t) e^{-i\Gamma\cos(\omega_1 t + \phi_1)}\right] \tag{10}$$

define $F_t[f(t)](\omega) = \hat{f}(\omega)$, and invoking the convolution theorem

$$\frac{h_0 e^{i\phi_0}}{\sqrt{2\pi}} \delta(\omega_c - \omega) = \hat{f}(\omega) \star F_t\left[e^{-i\Gamma\cos(\Omega t + \phi)}\right] \tag{11}$$

invoking the Jacobi-Anger Expansion which has the form []:

$$e^{iz\cos(\theta)} = \sum_{n=-\infty}^{\infty} e^{in\pi/2} J_n(z) e^{in\theta} \tag{12}$$

so equation (2) becomes

$$\frac{h_0 e^{i\phi_0}}{\sqrt{2\pi}} \delta(\omega - \omega_0) = \hat{f}(\omega) \star \mathcal{F}_t\left[\sum_{n=-\infty}^{\infty} e^{in\pi/2} J_n(-\Gamma) e^{in(\omega_1 t + \phi_1)}\right] \tag{13}$$

Bessel Functions have the properties

$$J_n(-z) = (-1)^n J_n(z) \tag{14}$$

so

$$\mathcal{F}_t\left[\sum_{n=-\infty}^{\infty} e^{in\pi/2} J_n(-\Gamma) e^{in(\omega_1 t + \phi_1)}\right] = \sum_{n=-\infty}^{\infty} (-1)^n e^{in\pi/2} e^{in\phi_1} J_n(\Gamma) \mathcal{F}_t\left[e^{in\omega_1 t}\right] \tag{15}$$

$$= \frac{1}{\sqrt{2\pi}} \sum_{n=-\infty}^{\infty} e^{in(\phi_1 - \pi/2)} J_n(\Gamma) \delta(\omega - n\omega_1) \tag{16}$$

where we have used $(-1)^n i^n = (-i)^n = e^{-in\pi/2}$, and the linearity of the Fourier Transform $F_t[f+g] = F_t[f] + F_t[g]$. The Fourier transform of this is

$$h_0 e^{i\phi_0} \delta(\omega - \omega_0) = \hat{f}(\omega) \star \left[\sum_{n=-\infty}^{\infty} e^{in(\phi_1 - \pi/2)} J_n(\Gamma) \delta(\omega - n\omega_1)\right] \tag{17}$$

so performing the convolution

$$\hat{f}(\omega) \star \delta(\omega - n\omega_1) = \int \hat{f}(\omega - \widetilde{\omega}) \delta(\widetilde{\omega} - n\omega_1) d\widetilde{\omega} \tag{18}$$

$$= \hat{f}(\omega - n\omega_1) \tag{19}$$

which brings us to the almost final answer:

$$h_0 e^{i\phi_0} \delta(\omega - \omega_0) = \sum_{n=-\infty}^{\infty} e^{in(\phi_1 - \pi/2)} J_n(\Gamma) \hat{f}(\omega - n\omega_1) \tag{20}$$

but for later convenience let's have $n \to -n$. We will use the other property of the Bessel Functions: []

$$J_{-n}(z) = (-1)^n J_n(z) \tag{21}$$

Which brings us to the Gustafson Algorithm (someone should check this out before we submit the paper):

$$h_0 e^{i\phi_0} \delta(\omega - \omega_0) = \sum_{n=-\infty}^{\infty} e^{-in(\phi_1 + \pi/2)} J_n(\Gamma) \hat{f}(\omega + n\omega_1) \tag{22}$$

This algorithm has been implemented in the past to demodulate the carrier frequency to recover the true amplitude [**?**].

This algorithm in its current form cannot be used on real data because it assumed a complex waveform. This assumption allowed for a clean demodulation, which is spoiled if one takes the real of this function. This is due to the nonlinearity (is this the correct term) of the real opperator as demonstrated by

$$\Re\{\cdot b\} \neq \Re\{a\} \cdot \Re\{b\} \tag{23}$$

We can use this algorithm as a guess as to find the form that will work with a real valued waveform. Upon comparison of the Fourier transforms of the complex and real waveforms (see appendix A and B) we see they are very similar. The real looks like the complex with an additional sum of mirrored terms (explain what I mean by this).

What would we have to do to get the fourier transform of the real to look exactly like the fourier transform of the complex wave? Unsurprisingly not much because they are such similar functions. We would only have to multiply each term by some phase factor to get the real fourier transform to look like the sum of two complex fourier transforms. After adding in the phase factors we plug the fourier transform of the real wave into the Gustafson Algorithm which will yeald two delta functions now instead of one (because the fourier transform of the real is the sum of two complex wave fourier transforms). One delta function will be at $+\omega_0$, this is the one of interest, and the other will be at $-\omega_0$. (A much more rigerous explanation of this is needed.) If we carry the search out over only positive values of ω_0 then we can throw out all terms in red of the fourier transform of the real wave because they are inconsequential to the algorithm. Finally, the phase terms that were added to the foureier transform of the real to make it look like the complex can be encorperated into the Guatafson Algorithm. The only remaining thing to do is multiply the Gustafson Algorithm by two (explain why).

A. Discussion of The Gustafson Algorithm

It is not explicitly obvious how The Gustafson Algorithm, Eq. 22, can be used as a search algorithm able to determin the values $\omega_0, \omega_1, \phi_0, \phi_1, \Gamma$. In this section we seek to make obvious what Eq. 22 can do.

Now let's assume that the data takes the form

$$f(t) = \Re\left\{ h_0 e^{i(\omega_0 t + \phi_0 + \Gamma \cos(\omega_1 t + \phi_1))} \right\} \tag{24}$$

but we do not know the values of $\omega_0, \omega_1, \phi_0, \phi_1, \Gamma$. To determin these values we will try the values $\widetilde{\omega}_0, \widetilde{\omega}_1, \widetilde{\phi}_1, \widetilde{\Gamma}$ in the Gustafson Algorithm

$$? = \sum_{n=-\infty}^{\infty} e^{-in(\widetilde{\phi}_1 + \pi/2)} J_n(\widetilde{\Gamma}) \hat{f}(\omega + n\widetilde{\omega}_1) \tag{25}$$

To see what this will yeald we substitute the Fourier Transform of the real of the waveform equation (B6), into the above equation

$$\frac{h_0}{2} \sum_{m,n=-\infty}^{\infty} e^{i(m\phi_1 - n\widetilde{\phi}_1)} J_n(\widetilde{\Gamma}) J_m(\Gamma)$$
$$\times \left[e^{i(\phi_0 + (m-n)\pi/2)} \delta(\omega - \omega_0 + n\widetilde{\omega}_1 - m\omega_1) + e^{-i(\phi_0 + (m+n)\pi/2)} \delta(\omega + \omega_0 + n\widetilde{\omega}_1 - m\omega_1) \right] \tag{26}$$

- If $\widetilde{\phi}_1 = \phi_1$ then this formula does not depend on ether $\widetilde{\phi}_1$ or ϕ_1.
Bessel functions have the property []

$$? = \sum_{n=-\infty}^{\infty} e^{-in(\widetilde{\phi}_1+\pi/2)} J_n(\widetilde{\Gamma}) \hat{f}(\omega + n\widetilde{\omega}_1) \tag{27}$$

Where δ_m is the Kronecker Delta. []

III.   CARSON'S RULE AND THE NYQUIST FREQUENCY

To see what this will yeald we substitute the Fourier Transform of the real of the waveform equation (B6), into the above equation

$$\frac{h_0}{2} \sum_{m,n=-\infty}^{\infty} e^{i(m\phi_1-n\widetilde{\phi}_1)} J_n(\widetilde{\Gamma}) J_m(\Gamma)$$
$$\times \left[e^{i(\phi_0+(m-n)\pi/2)} \delta(\omega - \omega_0 + n\widetilde{\omega}_1 - m\omega_1) + e^{-i(\phi_0+(m+n)\pi/2)} \delta(\omega + \omega_0 + n\widetilde{\omega}_1 - m\omega_1) \right] \tag{28}$$

This needs to be treated in cases.

Case 1: Let's consider the most likely case when $\omega \neq \omega_0$ and $\omega_1 \neq \widetilde{\omega}_1$. Let's examin the term $\delta(\omega-\omega_0+n\widetilde{\omega}_1-m\omega_1)$ in the above equation in detail. This delta function appears in the double sum and is a function of both m and n, so the $n\widetilde{\omega}_1 - m\omega_1$ is changing over the sums whereas the value $\omega - \omega_0$ is constant (not a function of m or n). This delta is non-zero only if

$$0 = \omega - \omega_0 + n\widetilde{\omega}_1 - m\omega_1 \tag{29}$$
$$\omega_0 - \omega = n\widetilde{\omega}_1 - m\omega_1 \tag{30}$$

This can happen twice or never. By the Euclidean Algorithm, the delta will only be non-zero if

$$\gcd(\widetilde{\omega}_1, \omega_1) = \omega_0 - \omega \tag{31}$$

If this is false then the sum is zero. If it is true then call the values for m and n that make it true $\pm m_o$ and $\mp n_o$. So then the sum is

Placeholder for equation

Case 2: Now consider the case when $\omega = \omega_0$ and $\omega_1 \neq \widetilde{\omega}_1$. The term $\delta(\omega-\omega_0+n\widetilde{\omega}_1-m\omega_1)$ will only be non-zero if

$$\widetilde{\omega}_1 = \frac{m}{n}\omega_1 \tag{32}$$

Again this can happen twice or never. If this is false then the sum is zero.

Placeholder for equation

Case 3: Now consider the case when $\omega \neq \omega_0$ and $\omega_1 = \widetilde{\omega}_1$. The term $\delta(\omega-\omega_0+n\widetilde{\omega}_1-m\omega_1)$ will only be non-zero if

$$\omega - \omega_0 = (n - m)\widetilde{\omega}_1 \tag{33}$$

Again this can happen twice or never. If this is false then the sum is zero.

Cases 1-3: In all of these cases

Case 4: Now consider the case when $\omega = \omega_0$ and $\omega_1 = \widetilde{\omega}_1$. The term $\delta(\omega-\omega_0+n\widetilde{\omega}_1-m\omega_1)$ will only be non-zero if $m = n$ which will happen an infinite number of times. The sum becomes

$$\frac{h_0}{2} e^{i\phi_0} \delta(0) \sum_{n=-\infty}^{\infty} e^{in(\phi_1-\widetilde{\phi}_1)} J_n(\widetilde{\Gamma}) J_n(\Gamma) \tag{34}$$

Case 4a: Now if we let $\Gamma = \widetilde{\Gamma}$ and $\phi_1 = \widetilde{\phi}_1$ then the sum becomes

$$\frac{h_0}{2}e^{i\phi_0}\delta(0)\sum_{n=-\infty}^{\infty}J_n^2(\Gamma) = \frac{h_0}{2}e^{i\phi_0}\delta(0) \tag{35}$$

So if we guess every search parameter correctly, $\omega = \omega_0$, $\omega_1 = \widetilde{\omega}_1$, $\Gamma = \widetilde{\Gamma}$, and $\phi_1 = \widetilde{\phi}_1$, then we recover the

IV. CARSON'S RULE AND THE NYQUIST FREQUENCY

In order too fully reconstruct the carrier frequency we would need to take an infinite sum over the sidebands. As this is impractical and unnecessary as many terms are insignificant, we need to find a way to limit the number of sidebands we are summing over. The first problem is locating the sidebands' characteristic frequency. There are infinite sideband frequencies and eventually they will be higher than the Nyquist frequency which will cause aliasing of the sideband frequency. The Nyquist frequency, ψ_N, is defined as the maximum frequency that can be accurately reconstructed and is equal to half of the sampling frequency, ψ_s.

$$\psi_N = \frac{1}{2}\psi_s \tag{36}$$

Any side band with a frequency of ψ_0 higher than the Nyquist frequency, but less than the sampling frequency, will be reconstructed with a frequency of $(\psi_s - \psi_0)$. That is the frequency will be under-sampled and an alias frequency will be produced. When this occurs the best case scenario is that the alias frequency is unique and does not correspond to the frequency of another lower frequency sideband. In this case we can use anti-aliasing techniques to correct for the aliasing and still obtain information about the amplitude and frequency of the higher side bands. The worst case scenario is that the aliased frequency is too close to another lower frequency sideband and this will cause two problems: a systematic error will be added to the measurement of the lower side band's amplitude, and we will be unable to determine the necessary information on what the amplitude of the higher frequency would be. To minimize the effect this might have we would like any sidebands with a frequency over the Nyquist frequency to have as low an amplitude as possible. For this we can employ Carson's rule. Carson's rule can be understood to say that almost all (roughly 98 percent) of the power for a frequency-modulated sinusoidal signal is contained within a finite bandwidth B_T, defined by:

$$B_T = 2(\Delta\psi + \psi_m) \tag{37}$$

where $\Delta\psi$ is the peak frequency deviation of the instantaneous frequency $\psi(t)$ from the center carrier frequency ψ_c, and ψ_m is the highest frequency in the modulating signal. In our case the highest frequency of the modulating signal is the carrier frequency, ψ_c. From this calculation we can adjust our sampling frequency to ensure it is large enough in order to minimize aliasing. This also puts a limit on the number of sidebands we need to sum over to just those that fall within the bandwidth. The important thing to take away from this is that it takes an infinite bandwidth to prefectly transmit a phase or frequency modulated wave, regardless of how smooth it is, but in practice only a finite bandwidth is needed for an accurate approximation.

$$B_T = 2(\Delta\psi + \psi_m) \tag{38}$$

where $\Delta\psi$ is the peak frequency deviation of the instantaneous frequency $\psi(t)$ from the center carrier frequency ψ_c, and ψ_m is the highest frequency in the modulating signal. In our case the highest frequency of the modulating signal is the carrier frequency, ψ_c. From this calculation we can adjust our sampling frequency to ensure it is large enough in order to minimize aliasing. This also puts a limit on the number of sidebands we need to sum over to just those that fall within the bandwidth. The important thing to take away from this is that it takes an infinite bandwidth to prefectly transmit a phase or frequency modulated wave, regardless of how smooth it is, but in practice only a finite bandwidth is needed for an accurate approximation.

V. ERROR ANALYSIS

While the search for monochromatic gravitational waves via the LIGO detector is relatively effortless, the adulteration of signals obtained from the detected by noise adds an appreciable number of complications to the problem.

By the same token, techniques by which improved resistance of the LIGO detector to noise can be obtained has been investigated [?] [?].

A. Noise Sources

Since the signal being searched for is relatively stable but of little amplitude, the reliability of data obtained from the detector is related to the degree of noise therein. Among others, quantum, thermal, seismic and Newtonian noise have been implicated as prime drivers of LIGO data adulteration. Since the prime noise contributor is quantum, a summation of all the noise sources are approximately Gaussian. Thus, it suffices to use the properties of Gaussian noise to understand the volatility of the data.

B. Noise Elimination

As mentioned previously, quantum noise — in particular, thermal noise — has been implicated as a limiting factor in the sensitivity of gravitational wave inteferometers and hence a prime factor in the degradation of the signal quality [5]. Following from this, it can be inferred that the distribution of the noise is approximately Gaussian.

By low-pass filtering or spectral subtraction, it is possible to derive signals with high SNR; however, these widely-accepted approaches require information which can be difficult to obtain. Since the frequency of the monochromatic wave being searched for is not known, low-pass filtering result in erroneous outputs. Spectral subtraction requires a sample of the noise; nevertheless, due to the low SNR of LIGO data, it is precarious to find segments with pure noise.

In this section, we introduce an alternate approach by which Gaussian noise in data may be reduced. This method utilizes the following principle: the nature of the noise is not known but the nature of the signal is known. Our methodology consists of subtracting estimated noise from the signal via singular value decomposition of intrinsic mode functions and assumes the noise is correlated across different channels.

1. Proposed denoising algorithm

In an effort to reduce the noise, we shall consider data from two channels. By the assumption that the noise observed is additive (and correlated), we yield the following:

$$\xi^{(1)}(t) = f^{(1)}(t) + \epsilon^{(1)}(t) \tag{39}$$

$$\xi^{(2)}(t) = f^{(2)}(t) + \epsilon^{(2)}(t) \tag{40}$$

where $\xi^{(n)}(t)$ is the data observed, $f^{(n)}(t)$ is the true signal and $\epsilon^{(n)}(t)$ is the noise obtained from the n-th channel (or gravitational wave interferometer) with $\epsilon^{(n)}(t) \sim \mathcal{N}(0, \sigma^2)$.

First, we disintegrate each observed signal into α intrinsic mode functions via empirical mode decomposition and arrange them into a $2\alpha \times T$ matrix $\mathbf{L}$:

$$\mathbf{L} = \begin{pmatrix} l^{(1)}_{1,t_1} & l^{(1)}_{1,t_2} & \cdots & l^{(1)}_{1,t_T} \\ l^{(1)}_{2,t_2} & l^{(1)}_{2,t_2} & \cdots & l^{(1)}_{2,t_T} \\ \vdots & \vdots & \vdots & \vdots \\ l^{(1)}_{\alpha,t_1} & l^{(1)}_{\alpha,t_2} & \cdots & l^{(1)}_{\alpha,t_T} \\ l^{(2)}_{\alpha+1,t_1} & l^{(2)}_{\alpha+1,t_2} & \cdots & l^{(2)}_{\alpha+1,t_T} \\ l^{(2)}_{\alpha+2,t_2} & l^{(2)}_{\alpha+2,t_2} & \cdots & l^{(2)}_{\alpha+2,t_T} \\ \vdots & \vdots & \vdots & \vdots \\ l^{(2)}_{2\alpha,t_1} & l^{(2)}_{2\alpha,t_2} & \cdots & l^{(2)}_{2\alpha,t_T} \end{pmatrix} \tag{41}$$

where $l^{(n)}_{p,t_q}$ is the $\left[\left((p-1)\mathrm{mod}\,\alpha\right)+1\right]$-th intrinsic mode function at time t_q of $\xi^{(n)}(t)$, and with T being the total number of data points observed.

Thereafter, the fast Fourier transform of each intrinsic mode function in $\mathbf{L}$ is computed to obtain a matrix $\mathcal{F}(\mathbf{L})$. Singular value decomposition of the variance-covariance matrix obtained from $\mathcal{F}(\mathbf{L})$ is then computed to result in the following:

$$\Sigma = \mathbf{USV} \tag{42}$$

where $\Sigma = T^{-1}\left[\mathcal{F}(\mathbf{L})^{\mathbf{T}} - \mathbf{11}^{\mathbf{T}}\mathcal{F}(\mathbf{L})^{\mathbf{T}}T^{-1}\right]^{\dagger}\left[\mathcal{F}(\mathbf{L})^{\mathbf{T}} - \mathbf{11}^{\mathbf{T}}\mathcal{F}(\mathbf{L})^{\mathbf{T}}T^{-1}\right]$ with $(\cdot)^{\mathbf{T}}$ being the transpose, the conjugate transpose $(\cdot)^{\dagger}$ and $\mathbf{1}$ a $T \times 1$ column matrix.

The fast Fourier transforms are de-correlated to form a matrix $\mathbf{R}$ by employing the following:

$$\mathbf{R} = \mathbf{U}^{\mathbf{T}}\mathbf{L} \tag{43}$$

After the de-correlation procedure above, we seek to apply a threshold Δ which dictates the approximate percentage of statistically irrelevant information about the Fourier transform we shall discard. Prior to the thresholding procedure, the eigenvectors that contribute to approximately Δ percent of the variance of the transform by virtue of their respective eigenvalues is estimated using the following procedure:

$$y = \underset{b}{\operatorname{argmin}}\left(\left|\frac{\sum_{j=1}^{(b)}\lambda_j}{trace\{\mathbf{S}\}} - \frac{\Delta}{100}\right|\right) \tag{44}$$

where y is the index denoting the yth eigenvalue from λ_y with $\lambda = diag(\mathbf{S})$.

To apply the threshold, the projections with eigenvalues whose indices are less than y are retained and the rest are replaced with zero row vectors:

$$\mathbf{R}_r = \begin{cases} \mathbf{R}_r & ,r < y \\ \mathbf{0} & ,r \geq y \end{cases}$$

where $\mathbf{R}_r$ the rth row of the matrix $\mathbf{R}$.

The fast Fourier transforms are then re-correlated to obtain denoised intrinsic mode functions in the following manner:

$$\tilde{\mathbf{L}} = \mathbf{VR} \tag{45}$$

The real component of the inverse fast Fourier transform of each row of $\tilde{\mathbf{L}}$ is then computed to obtain a matrix $\mathbf{D}$ of similar architecture with denoised intrinsic mode functions. Thereafter, the reconstructed signals $\xi^{\hat{(n)}}(t)$ are obtained as follows:

$$\xi^{\hat{(n)}}(t_q) = \sum_{u=(n-1)\alpha+1}^{n\alpha} \mathbf{d}_{u,q} \tag{46}$$

where $\mathbf{d}_{u,q}$ is the value at the uth row and q^{th} column of $\mathbf{D}$.

2. Discussion

In contrast with denoising techniques such as low-pass filtering, this approach does not require the knowledge of the highest frequency of the signal being recorded. However, the knowledge of how much variance of the data to keep is integral to successful denoising — this is usually unknown and techniques have been proposed to solve this non-trivial problem [].

VI. IMPLEMENTING THE GUSTAFSON ALGORITHM IN C++

A. Calculating Bessel Functions

Known problems with the algorithm include calculating large order bessel functions. The bessel functions of natural number order are given by
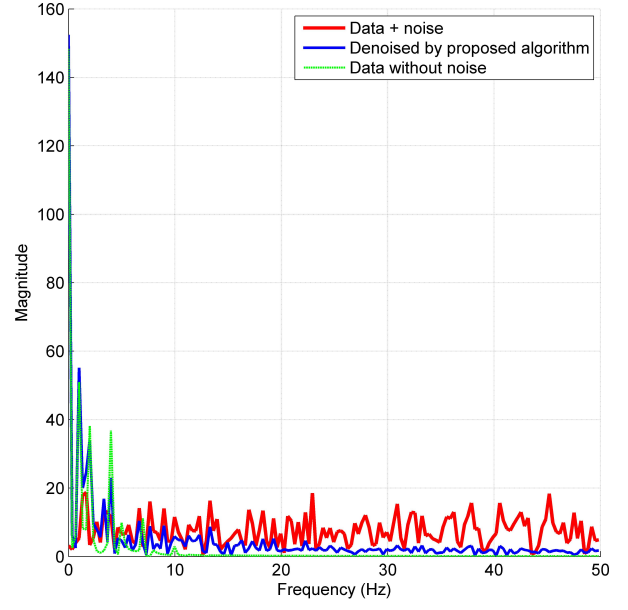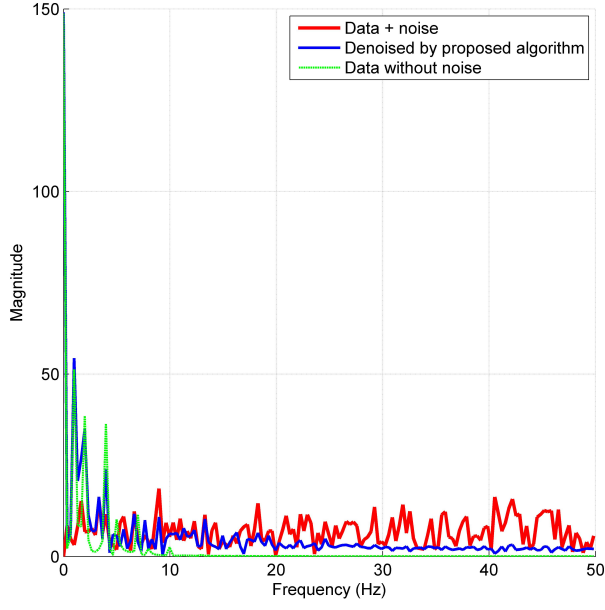
(a) Fourier transform of the proposed denoising approach on channel 1.

(b) Fourier transform of the proposed denoising approach on channel 2.

FIG. 2: Output of the proposed denoising approach on two channels with signals of similar frequency modulation, but shifted in time. This procedure assumes the signal being recorded is from the same source and the noise observed in each channel are correlated.
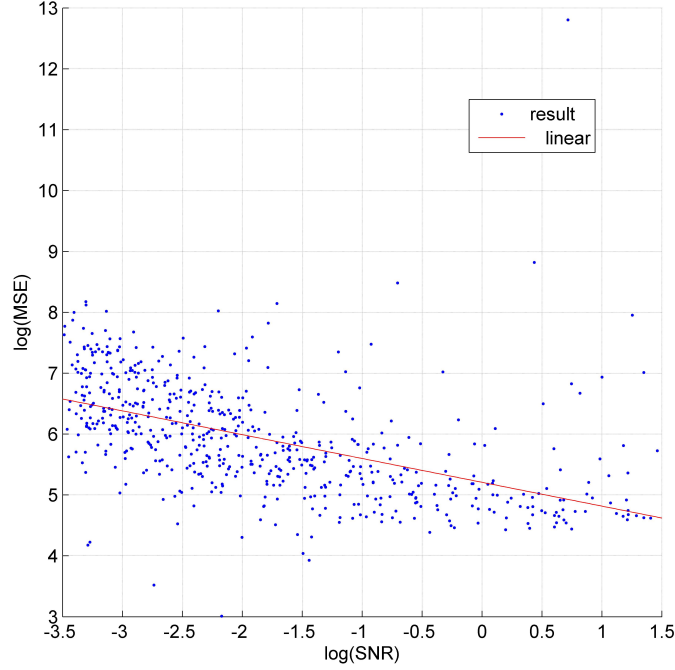

FIG. 3: Denoising results

$$J_n(z) = \sum_{m=0}^{\infty} \frac{(-1)^n}{m!(m+n)!} \left(\frac{z}{2}\right)^{2m+n} \tag{47}$$

so calculating the nth Bessel function involves calculating factorials greater than n!. The highest n for which we can store n! in an unsigned long integer type, the largest positive integer type, is 20:

$$2^{64} - 1 = 18,446,744,073,709,551,615 \tag{48}$$

$$< 21! = 51,090,942,171,709,440,000 \tag{49}$$

if we are willing to sacrafise some precision to truncation we can use a double precision floating point integer which allows values upto $1.797,693,134,862,315,7 \cdot 10^{308}$

$$170! \approx 7.25 \cdot 10^{306} < 1.797,693,134,862,315,7 \cdot 10^{308} < 171! \approx 1.24 \cdot 10^{309} \tag{50}$$

This is not acceptable hovever, because $|J_n(z)| \leq 1$, so when performing the sum we need precision all the way down to at the very least 0.1, which would require a mantissa with roughly 308 digits. This is not only impracticle, but it is by far one of the slowest ways one could calculate values of the Bessel functions. This whole buiseness of wresteling with factorials can be avoided by calculating the Bessel Functions using Bessel's Equation 51 [3].

$$x^2 J_n''(x) + x J_n'(x) + (x^2 - n^2) J_n(x) = 0 \tag{51}$$

The standard perscription for numerically solving differential equations is first to discretize the independent variable $x \to x_i = x_{min} + i \cdot \delta x$. Then use the limit definitions of the derivatives; we will use the three point definitions because their error goes as $O(\delta x^2)$ rather than using the two point definition with an error that goes as $O(\delta x)$ [?]. Also, because there are only one order of Bessel Functions in Bessel's Equation, the order is implied by the n that appears, so we will drop the subscript of n, $J_n \to J$, and we will further adopt the notation $J(x_i) = J_i$.

$$J_i' = \frac{J_{i+1} - J_{i-1}}{2\delta x} \tag{52}$$

$$J_i'' = \frac{J_{i-1} - 2J_i + J_{i+1}}{\delta x^2} \tag{53}$$

So the discretized form of Bessel's Equation is

$$x_i^2 \frac{J_{i-1} - 2J_i + J_{i+1}}{\delta x^2} + x \frac{J_{i+1} - J_{i-1}}{2\delta x} + (x^2 - n^2) J_i = 0 \tag{54}$$

$$\left(\frac{x_i^2}{\delta x^2} - \frac{x_i}{2\delta x} \right) J_{i-1} + \left(\left(1 - \frac{2}{\delta x^2} \right) x_i^2 - n^2 \right) J_i + \left(\frac{x_i^2}{\delta x^2} + \frac{x_i}{2\delta x} \right) J_{i+1} = 0 \tag{55}$$

Where we have collected like terms of J_i. For convenience we define coefficients to simplify the above equation.

$$a_i = \frac{x_i^2}{\delta x^2} - \frac{x_i}{2\delta x} \tag{56}$$

$$b_i = \left(1 - \frac{2}{\delta x^2} \right) x_i^2 - n^2 \tag{57}$$

$$c_i = \frac{x_i^2}{\delta x^2} + \frac{x_i}{2\delta x} \tag{58}$$

These coefficients can be simplified by using the definition for x_i, and taking $x_{min} = 0$.

$$a_i = i \left(i - \frac{1}{2} \right) \tag{59}$$

$$b_i = i^2 \left(\delta x^2 - 2 \right) - n^2 \tag{60}$$

$$c_i = i \left(i + \frac{1}{2} \right) \tag{61}$$

So the discretized Bessel equation with simplified coefficients is

$$a_i J_{i-1} + b_i J_i + c_i J_{i+1} = 0 \tag{62}$$

Wrighting out the system of equations explicitly:

$$b_1 J_1 + c_1 J_2 = -a_1 J_0 \tag{63}$$
$$a_2 J_1 + b_2 J_2 + c_2 J_3 = 0 \tag{64}$$
$$a_3 J_2 + b_3 J_3 + c_3 J_4 = 0 \tag{65}$$
$$\vdots \tag{66}$$
$$a_{n-1} J_{n-2} + b_{n-1} J_{n-1} + c_{n-1} J_n = 0 \tag{67}$$
$$a_n J_{n-1} + b_n J_n = -c_n J_{n+1} \tag{68}$$

Which suggests Bessel Equation be written as a matrix equation.

$$
\begin{pmatrix}
b_1 & c_1 & & & & \\
a_2 & b_2 & c_2 & & & \\
& a_3 & b_3 & c_3 & & \\
& & \vdots & \vdots & & \\
& & a_{n-1} & b_{n-1} & c_{n-1} \\
& & & a_n & b_n
\end{pmatrix}
\begin{pmatrix}
J_1 \\ J_2 \\ J_3 \\ \vdots \\ J_{n-1} \\ J_n
\end{pmatrix}
=
\begin{pmatrix}
-a_1 J_0 \\ 0 \\ 0 \\ \vdots \\ 0 \\ -c_n J_{n+1}
\end{pmatrix}
\tag{69}
$$

This is a tridiagonal matrix system that charactorized a one dimentional differential equation. It can be easilly solved using the standard Thomas Algorithm. To program this in C++ we need all the arrays to be indexed from 0, so

$$
\begin{pmatrix}
B_0 & C_0 & & & & \\
A_1 & B_1 & C_1 & & & \\
& A_2 & B_2 & C_2 & & \\
& & \vdots & \vdots & & \\
& & A_{N-4} & B_{N-4} & C_{N-4} \\
& & & A_{N-3} & B_{N-3}
\end{pmatrix}
\begin{pmatrix}
J_1 \\ J_2 \\ J_3 \\ \vdots \\ J_{N-3} \\ J_{N-2}
\end{pmatrix}
=
\begin{pmatrix}
-A_0 J_0 \\ 0 \\ 0 \\ \vdots \\ 0 \\ -C_{N-3} J_{N-1}
\end{pmatrix}
\tag{70}
$$

$$A_i = a_{i+1} = (i+1)\left(i + \frac{1}{2}\right) \tag{71}$$

$$B_i = b_{i+1} = (i+1)^2 \left(\delta x^2 - 2\right) - n^2 \tag{72}$$

$$C_i = c_{i+1} = (i+1)\left(i + \frac{3}{2}\right) \tag{73}$$

1.   The Thomas Algorithm

The Thomas Algorithm is a lightning fast way to solve tridiagonal systems like equation 70. The algorithm consists of two steps. First there is a forward substitution which eliminates the A_i's, and modifies the B_i's and the vector on the right which we will call the source vector S_i; $\forall i \in [0, N-3]$.

$$R_i = R_i - \frac{A_i}{B_{i-1}} R_{i-1}; \qquad \forall i \in [1, N-3] \tag{74}$$

$$B_i \rightarrow B_i - \frac{A_i}{B_{i-1}} C_{i-1}; \qquad \forall i \in [1, N-3] \tag{75}$$

$$S_i \rightarrow S_i - \frac{A_i}{B_{i-1}} S_{i-1}; \qquad \forall i \in [1, N-3] \tag{76}$$

Then there is a backwards substitution eliminating the C_i's, again modifying the S_i's. Finally we solve for J_i.

$$R_i = R_i - \frac{C_i}{B_{i+1}} R_{i+1}; \qquad \forall i \in [N-4, 0] \tag{77}$$

$$S_i \to S_i - \frac{C_i}{B_{i+1}} S_{i+1}; \qquad \forall i \in [N-4, 0] \tag{78}$$

$$J_i = \frac{S_{i-1}}{B_{i-1}}; \qquad \forall i \in [N-2, 1] \tag{79}$$

The time it takes to perform the Thomas Algorithm goes as N [].

2. Boundary Conditions

To solve this second-order differential equation we will need two boundary conditions. The boundary condition at $x = 0$ is simple.

$$J_n(0) = \begin{cases} 1 & : n = 0 \\ 0 & : n \neq 0 \end{cases}$$

For the other boundary condition we *could* use the asymtotic form of the Bessel functions. Theorem 5.1 in [3] states:

For each $n \in N$ there is a constant $C_n \in R$ such that, if $x \geq 1$, then

$$\left| J_n(x) - \sqrt{\frac{2}{\pi x}} \cos\left(x - \frac{\pi}{4}(2n+1)\right) \right| \leq \frac{C_n}{x^{3/2}} \tag{80}$$

This is an asymptotic expansion, so it is only valid for large values of x. It turns out the accuracy of the solution to bessels equation relies heavilly on the accuracy of the endpoint at $x \neq 0$. Figures 4a and 4b illistrate this point quite well. The conclusion is that the asymtotic form of the bessel functions is not accurate enough for even fairly large valuse of z. We can also do

$$J_n(z) = \frac{1}{\pi} \int_0^\pi \cos\left[z \sin\theta - n\theta\right] d\theta \tag{81}$$

Which is computed using a Riemann Sum

$$J_n(z) \approx \frac{1}{N} \sum_{i=0}^{N+1} \cos\left[z \sin(i \cdot dx) - n \cdot i \cdot dx\right]; \qquad dx = \frac{\pi}{N} \tag{82}$$

The function being integrated becomes more oscillitory as n increases. Numerical analysis shows that n gives the number of zeros the function has on the interval $(0, \pi)$ for $z = 0$. For $n = 0$ the number of zeros is given by $Floor(\frac{2z}{\pi})$. We want a way to ensure the calculation is accurate regardless of how oscillatory it is, but we also want it to be as fast as possible, so we use these facts regarding the zeros to ensure there are roughly the same number of integration points between zeros. By taking the number of (evenly spaced) integration points to be

$$N = 100 \cdot (n+1) \cdot Floor\left(\frac{2z}{\pi} + 1\right) \tag{83}$$

we acheved excellent results (accurate consistantly to 16 decimal places) for a wide range of z and n. The +1's are to ensure accurate results when z or n are zero. The algorithm can have problems when J is extremely small. Then the function can be off by many orders of magnitude, but because it is essentially zero, it does not seem to effect our results when used as a boundary condition for solving Bessel's Differential Equation.
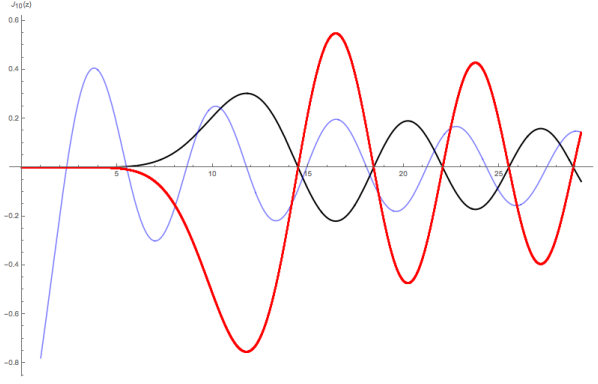
(a) Notice how the asymtotic form and the one calculated by our differential equation solver match up at the maximum value for z, but do not match up with the true solution. This has far reaching consequences. Whatever multiplicative factor the endpoint is off by seems to carry through for every other point. In this case the multiplicative factor (asymtotic / true) is almost exactly -2.5. Notice how this inverts the solution and makes it 250% larger.
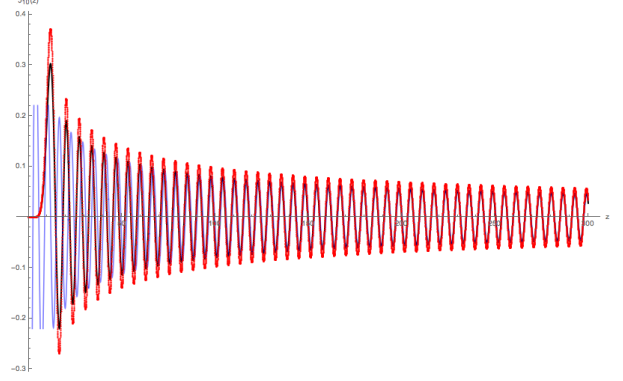
(b) For much larger values of z the asymtotic form is a better approximation to the true value. In this case the multiplicative factor (asymtotic / true evaluated at $z = 300$) is roughly 1.2 which results in the soultion being roughly 20% larger than it should be.

FIG. 4: The blue curve is the asymtotic form of the bessel functions as given in equation 80, the black curve is $J_{10}(x)$ as given by Mathematica, and the red curve is the one calculated by our differential equation solver. Note, both of these solutions were calculated using 10,000 points. Even though the solution in figure 4a has 10 times the point density, it is limited in accuracy by the endpoint!

Parameters	Point by Point Using Integral	Thomas Algo. Solving Bessel's Equation	Speed Increse
$n = 3$ $N = 500$ $z_{max} = 20.0$	0.051786 s	0.00013800 s	375
$n = 14$ $N = 50,000$ $z_{max} = 100.0$	113.33 s	0.003937 s	28,785

TABLE I: N is the number of points returned, n is the order of the bessel function, and the points calculated were for $z \in [0, z_{max}]$

3. Calculating Bessel Functions: Results

The ultimate benchmark for sucess in calculating Bessel Functions in this manner (using the Thomas Algorithm to solve Bessel's Differential Equation) is to compare it to the stardard way of calculating the value at each point using the Riemann Sum (as defined in equation 82 section VI A 2). So how much faster is it? This depends on the values of n and z because we use a dynamic number of integration points as given by eq. 83. Table I gives the speed increse for various parameters.

Table 5 gives three examples of Bessel Functions that were calculated using the Thomas Algorithm to solve Bessel's Equation.

VII.   CONCLUSION

Recap the benifits of working in the frequency domain vs the time domain. It is the belief of this author that the methods outlined in this paper are unlikely to be useful for searching for gravitational waves.
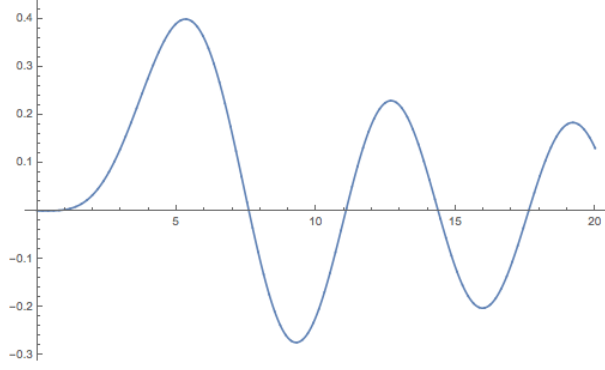
(a) n=4, numPts=10,000, xMax=20, comptime=0.00082
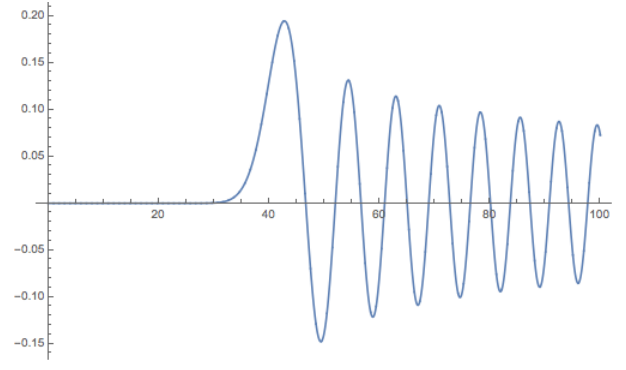
(b) n=40, numPts=10,000, xMax=100, comptime=0.00092
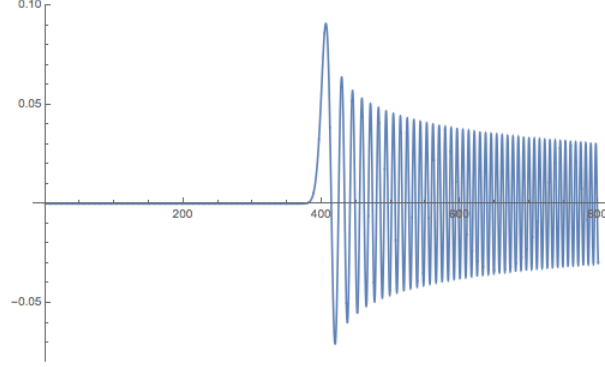
(c) n=400, numPts=10,000, xMax=800, comptime=0.00200;
About half the computation time went to calculating the
endpoint!

FIG. 5

Appendix A: The Fourier Transform of The Complex Function

I BELIEVE I FORGOT SOME FACTORS OF 2PI HERE!! Use the convolution theorem Use the Jacobi-Anger expansion 12 Use the linearity of the Fourier Transform Use the linearity of the Convolution

$$\mathcal{F}_t\left[h_0 e^{i(\omega_0 t + \phi_0 + \Gamma\cos(\omega_1 t + \phi_1))}\right] = h_0 e^{i\phi_0}\mathcal{F}_t\left[e^{i\omega_0 t}e^{i\Gamma\cos(\omega_1 t + \phi_1)}\right] \tag{A1}$$

$$= h_0 e^{i\phi_0}\mathcal{F}_t\left[e^{i\omega_0 t}\right]\star\mathcal{F}_t\left[e^{i\Gamma\cos(\omega_1 t + \phi_1)}\right] \tag{A2}$$

$$= h_0 e^{i\phi_0}\delta(\omega - \omega_0)\star\mathcal{F}_t\left[\sum_{n=-\infty}^{\infty}e^{in\pi/2}J_n(\Gamma)e^{in(\omega_1 t + \phi_1)}\right] \tag{A3}$$

$$= h_0 e^{i\phi_0}\delta(\omega - \omega_0)\star\sum_{n=-\infty}^{\infty}e^{in\pi/2}e^{in\phi_1}J_n(\Gamma)F_t\left[e^{in\omega_1 t}\right] \tag{A4}$$

$$= h_0 e^{i\phi_0}\delta(\omega - \omega_0)\star\sum_{n=-\infty}^{\infty}e^{in(\phi_1 + \pi/2)}J_n(\Gamma)\delta(\omega - n\omega_1) \tag{A5}$$

$$= h_0 e^{i\phi_0}\sum_{n=-\infty}^{\infty}e^{in(\phi_1 + \pi/2)}J_n(\Gamma)\delta(\omega - \omega_0)\star\delta(\omega - n\omega_1) \tag{A6}$$

$$= h_0 e^{i\phi_0}\sum_{n=-\infty}^{\infty}e^{in(\phi_1 + \pi/2)}J_n(\Gamma)\delta(\omega - \omega_0 - n\omega_1) \tag{A7}$$
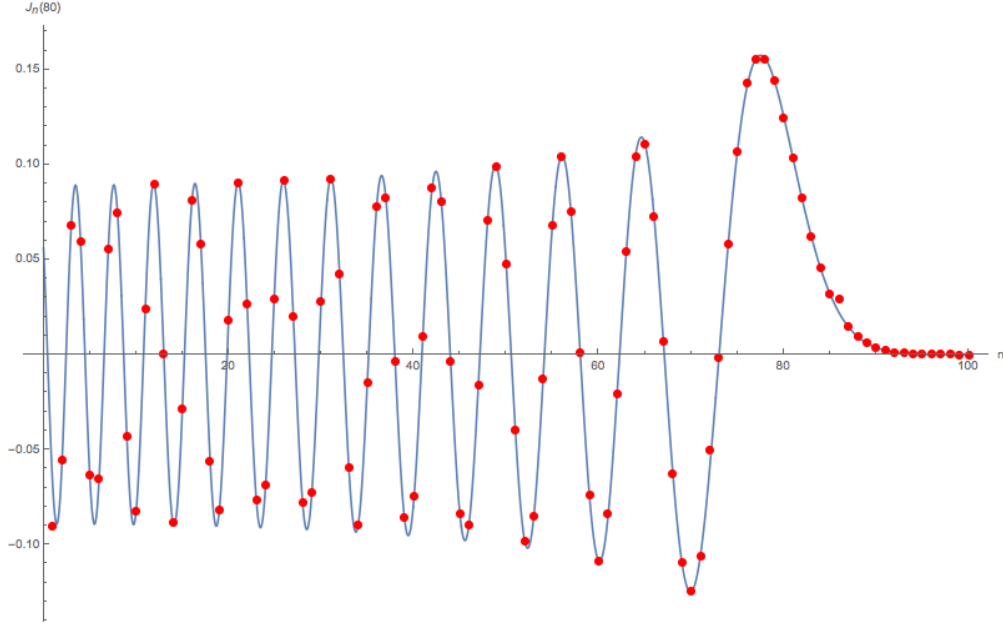
FIG. 6: This plot is a plot of $J_n(80)$ for values of $n \in (0, 100)$. The blue curve was generated by the BesselJ function of Mathematica. The red dots were calculated by my code. The two sets of data are in excelent agreement at except perhaps $n = 0, 85$ in which case there is a slight disagreement. This is a small selection of the $400,000$ data points my code generated in 0.33 seconds (on 5 year old a loptop). It solved the Bessel differential equation for 4000 steps in $\Gamma \in (0, 100)$, then saves the output, and moved on to solve Bessel's Equation for the next value of n until all values of Γ and n were solved for.

Appendix B: The Fourier Transform of The Real-Valued Function

$$\mathcal{F}_t\left[\Re\left\{h_0 e^{i(\omega_0 t+\phi_0+\Gamma\cos(\omega_1 t+\phi_1))}\right\}\right] = \frac{1}{2}\mathcal{F}_t\left[h_0 e^{i(\omega_0 t+\phi_0+\Gamma\cos(\omega_1 t+\phi_1))} + h_0 e^{-i(\omega_0 t+\phi_0+\Gamma\cos(\omega_1 t+\phi_1))}\right] \tag{B1}$$

$$= \frac{h_0}{2}\left[e^{i\phi_0}\mathcal{F}_t\left[e^{i(\omega_0 t+\Gamma\cos(\omega_1 t+\phi_1))}\right] + e^{-i\phi_0}\mathcal{F}_t\left[e^{i(-\omega_0 t-\Gamma\cos(\omega_1 t+\phi_1))}\right]\right] \tag{B2}$$
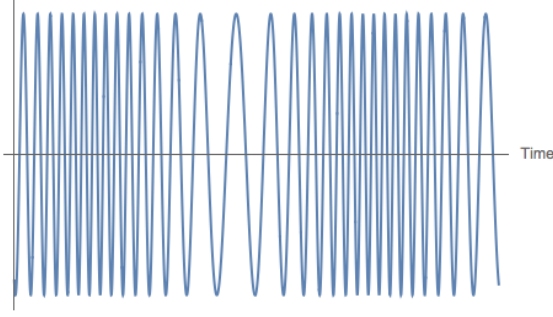
From the previous section we see that
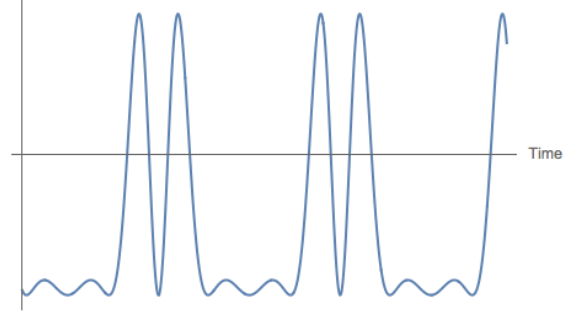
$$\mathcal{F}_t\left[e^{i(\omega_0 t+\Gamma\cos(\omega_1 t+\phi_1))}\right] = \sum_{n=-\infty}^{\infty} e^{in(\phi_1+\pi/2)} J_n(\Gamma)\delta(\omega-\omega_0-n\omega_1) \tag{B3}$$

and by replacing ω_0 with $-\omega_0$ and Γ with $-\Gamma$, and using the fact that $J_n(-\Gamma) = (-1)^n J_n(\Gamma)$ we also have

$$\mathcal{F}_t\left[e^{i(-\omega_0 t-\Gamma\cos(\omega_1 t+\phi_1))}\right] = \sum_{n=-\infty}^{\infty} e^{in(\phi_1-\pi/2)} J_n(\Gamma)\delta(\omega+\omega_0-n\omega_1) \tag{B4}$$

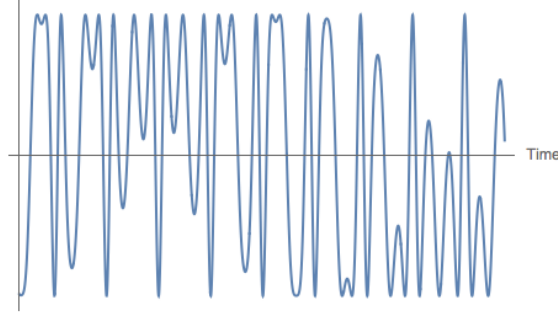so the Fourier Transform of the real part of our frequency/phase modulated signal is

(a) A "nice" signal that is what comes to mind for cyclic frequency modulated signals.
$\Gamma = 9.88, \omega_0 = 3.62, \omega_1 = 0.21, \phi_1 = 3.14$

(b) One example of the exotic signals cyclic frequency modulation can produce.
$\Gamma = 2.88, \omega_0 = 1.5, \omega_1 = 0.75, \phi_1 = 0$

(c) A particularly nasty waveform that could be mistaken as noise by looking at it. $\Gamma = 3, \omega_0 = 0.42, \omega_1 = 0.46, \phi_1 = 0.1$

$$
\mathcal{F}_t\left[\Re\left\{h_0 e^{i(\omega_0 t + \phi_0 + \Gamma\cos(\omega_1 t + \phi_1))}\right\}\right] = \frac{1}{2}h_0\left[e^{i\phi_0}\sum_{n=-\infty}^{\infty}e^{in(\phi_1+\pi/2)}J_n(\Gamma)\delta(\omega-\omega_0-n\omega_1)\right.
$$
$$
\left. + e^{-i\phi_0}\sum_{n=-\infty}^{\infty}e^{in(\phi_1-\pi/2)}J_n(\Gamma)\delta(\omega+\omega_0-n\omega_1)\right]
$$
$$
= \frac{1}{2}h_0\sum_{n=-\infty}^{\infty}e^{in\phi_1}J_n(\Gamma)\left[e^{i(\phi_0+n\pi/2)}\delta(\omega-\omega_0-n\omega_1)\right.
$$
$$
\left. + e^{-i(\phi_0+n\pi/2)}\delta(\omega+\omega_0-n\omega_1)\right]
$$

(B5)

$$
\hat{f}(\omega) = \frac{1}{2}h_0\sum_{n=-\infty}^{\infty}e^{in\phi_1}J_n(\Gamma)\left[e^{i(\phi_0+n\pi/2)}\delta(\omega-\omega_0-n\omega_1) + e^{-i(\phi_0+n\pi/2)}\delta(\omega+\omega_0-n\omega_1)\right]
$$

(B6)

Notice that, by taking the fourier transform of just the real part of our frequency modulated function it has added the terms in red. (Go into more detail why that is) The other important change is that the X_n and Y_n terms were added (Again, go into more detail why that is).

Appendix C: Selected Waveforms

[1] Deanna Emery. A coherent three dimensional fft based search method for gravitational wave from neutron star systems. *LIGO DCC*, (T1500307-v2), September 2015.

[2] BP Abbott et al. (LIGO Scientific Collaboration and Virgo Collabor...

binary black hole merger. *Physical Review Letters*, 116(061102):1–16, 12 February 2016.

[3] Gerald B. Folland. *Fourier Analysis and its Applications.* Number ISBN 0-534-17097-3. Brooks and Cole Publishing Company, 1992.

[4] David J. Griffiths. *Introduction to Quantum Mechanics.* Number ISBN 0-13-111892-7. Pearson, second edition edition, 2005.

[5] Peter R. Saulson. *Fundamentals of Interferometric Gravitational Wave Detectors.* World Scientific Publishing Company, March 31, 1994.